Article

A Diagram of Structure Evolution of $Pb(Zn_{1/3}Nb_{2/3})O_3$-9%$PbTiO_3$ Relaxor Ferroelectric Crystals with Excellent Piezoelectric Properties

Hua Zhou[1,2], Tao Li[1,2,3], Nian Zhang[4], Manfang Mai[1,2], MaoYe[1,2], Peng Lin[1], Chuanwei Huang[1], Xierong Zeng[1,2], Haitao Huang[3] and Shanming Ke[1,*]

[1] College of Materials Science and Engineering and Shenzhen Key Laboratory of Special Functional Materials, Shenzhen University, Shenzhen 518060, China; zhouhua3612@163.com (H.Z.); litao@fjirsm.ac.cn (T.L.); mfmai1121@hotmail.com (M.M.); kfadn0125@gmail.com (M.Y.); lin.peng@szu.edu.cn (P.L.); cwhuang@szu.edu.cn (C.H.); zengxier@szu.edu.cn (X.Z.)

[2] College of Optoelectronic Engineering and Key Laboratory of Optoelectronic Devices and Systems of Ministry of Education and Guangdong Province, Shenzhen University, Shenzhen 518060, China

[3] Department of Applied Physics and Materials Research Centre, The Hong Kong Polytechnic University, Hung Hom, Kowloon, Hong Kong; aphhuang@polyu.edu.hk (H.H.)

[4] Center for Excellence in Superconducting Electronics, Shanghai Institute of Microsystem and Information Technology, Chinese Academy of Sciences, 865 Changning Road, Shanghai 200050, China; zhangn@mail.sim.ac.cn (N.Z.)

* Correspondence: smke@szu.edu.cn; Tel.: +86-755-2653-4059.

Abstract: Piezoelectric properties are of significant importance to medical ultrasound, actuators, sensor, and countless other device applications. The mechanism of piezoelectric properties can be deeply understood from structure evolutions. In this paper, we report a diagram of structure evolutions of the $Pb(Zn_{1/3}Nb_{2/3})_{0.91}Ti_{0.09}O_3$ (PZN-9PT) single crystal with excellent piezoelectric properties among the orthorhombic, tetragonal, and cubic phases with temperature increasing from room temperature to 220 °C. Through fitting the temperature dependence XRD curves with Gauss and Lorenz functions, we obtained the evolutions of the content ratio of three kinds of phases (orthorhombic, tetragonal and cubic) and the lattice parameters of the PZN-9PT system with the changes of temperature. The XRD fitting results together with Raman and dielectric spectrums show that the phase transitions of PZN-9PT are a typical continuous evolution process. Additionally, resonance and anti-resonance spectrum show excellent piezoelectric properties of the crystals, which probably originate from the nano twin domains, as demonstrated by the TEM images. Of particular attention is that the thickness electromechanical coupling factor k_t is up to 72%.

Keywords: $Pb(Zn_{1/3}Nb_{2/3})O_3$-9%$PbTiO_3$; relaxor ferroelectric crystals; structure phase transition; electromechanical coupling factor.

1. Introduction

Since Kuwata et al. [1] first reported that the solid solutions of rhombohedral lead zinc niobate, $Pb(Zn_{1/3}Nb_{2/3})O_3$ (PZN), and tetragonal lead titanate, $PbTiO_3$ (PT), have a morphotropic phase boundary (MPB) near 9 mol% PT, PZN-PT has attracted much exclusive attention due to its excellent and unique properties. Recently, Zhang *et al.* and Sun *et al.* [2-4] demonstrated that the $Pb(Zn_{1/3}Nb_{2/3})_{0.91}Ti_{0.09}O_3$ (PZN-9PT) crystal exhibits an exceptionally large piezoelectric constant (d_{33} > 2000 pC/N) and electromechanical coupling factor in longitudinal bar mode (k_{33} > 92%). These properties are expected to be applied in high-quality piezoelectric devices, such as medical ultrasonic transducers, actuators, and sonars, as replacements for conventional PZT ceramics [4-7]. In the PZN-9PT crystal system, different from the normal ferroelectric (e.g. PT) [8] with a long coherent length of order, the random distribution of B-ions (here, B represents Zn, Nb and Ti atoms)

prevents the formation of the long range ferroelectric order [8,9]. Additionally, the charge and ionic radius differences are of great importance for the relaxor ferroelectric (RFE) properties, because they directly determine the degree of order in the B-ion sublattice and then the coherence length of order [10-11]. Consequently, the phase diagram of the $Pb(B'B'')O_3$-$PbTiO_3$ systems are often more complex than the normal ferroelectrics. Through the X-ray diffraction (XRD), neutron diffraction, Raman spectrum, etc., many literatures had reported the evolution diagram of the (1-x)PZN-xPT phase transition with the change of x and temperature [12-15]. In spite of the intensive studies, their microscopic mechanisms, such as the ferroelectric phase transition in relaxor ferroelectrics, remain poorly understood. Moreover, the ratios among the different phases as the change of the system temperature are always seem to be ignored by researchers, which should play an important role in understanding the phase transition mechanism.

In order to reveal the evolutions of the phase structure driven by the temperature, we have successfully grown PZN-9PT single crystals by controlled top-seeded solution growth (TSSG) method. Of particular importance is that the TSSG technique offers some advantages in growing single crystals of good quality, low compositional segregation, and controllable morphology. Structure phase transition was observed by the in-situ variable temperature XRD, dielectric spectrum, Raman spectra. The resonance and anti-resonance spectrum showed that the PZN-9PT crystal exhibits excellent piezoelectric response, which probably originates from the nano twin structures in the PZN-9PT single crystal, as demonstrated by the transmission electron microscopy (TEM).

2. Results and Discussion

2.1. Structure phase transition of PZN-9PT crystals

It is universally acknowledged that PZN-9PT single crystals have five structure phases: monoclinic (M_C), rhombohedral (R), orthorhombic (O), tetragonal (T) and cubic (C), corresponding to their space groups: *Pm C*, *R3m*, *Amm2*, *P4mm*, and *Pm-3m*, respectively. PZN-9PT single crystals often possess the coexistent phase structures at the room temperature. Ye et al. [16] and Chang et al. [17] reported the coexistence of R-phase and T-phase in PZN-9PT single crystals at the room temperature. Later, Cox et al. [11-12] argued that the room temperature structure of PZN-9PT should be O-phase coexisting with T-phase. Generally speaking, for R-phase, the lattice parameters a=b=c, $\alpha=\beta=\gamma\neq90°$ (but nearly equal to 90° for PZN-9PT system), and for O-phase, $a\neq b\neq c$, $\alpha=\beta=\gamma=90°$. Based on these characteristics, we can distinguish the co-phase structures according to the XRD peak numbers of the {200} lattice plane. Figure 1(a) presents the survey of the variable temperature XRD patterns of powders made from the PZN-9PT relaxor ferroelectric single crystal. According to the changes of the XRD peak number for the families of the PZN-9PT lattice plane: {100}, {110}, {200}, {112} and {220}, etc, it is inferred that structure phase transitions occur at about 80 °C and 150 °C for the powders of PZN-9PT. The color curve lines in Figure 1(a) show the calculated XRD patterns for the pure phases of PZN-9PT powders through using Poudrix software. The {002} plane families for pure R-phase and O-phase display one peak and three peaks, respectively, as shown in Figure 1(b). The peak number of the experimental {200} result at room temperature is more than 3, indicating that PZN-9PT is not a pure O-phase at room temperature. Comparing with the simulated results (shown by color lines in Figure (a) and (b)), it is speculated that the phase of single crystal PZN-9PT should be composed of O- and T-phase. This observation is well consistent with the reports by Uesu *et al.* [18]. In addition, when the temperature rises to 150 °C or above, the peaks of {200} seem to merge into a single one, indicating the phase evolution from tetragonal/orthorhombic to cubic, as illustrated by the changes of blue and violet areas.

Peer-reviewed version available at Crystals 2017, 7, , 130; doi:10.3390/cryst7050130

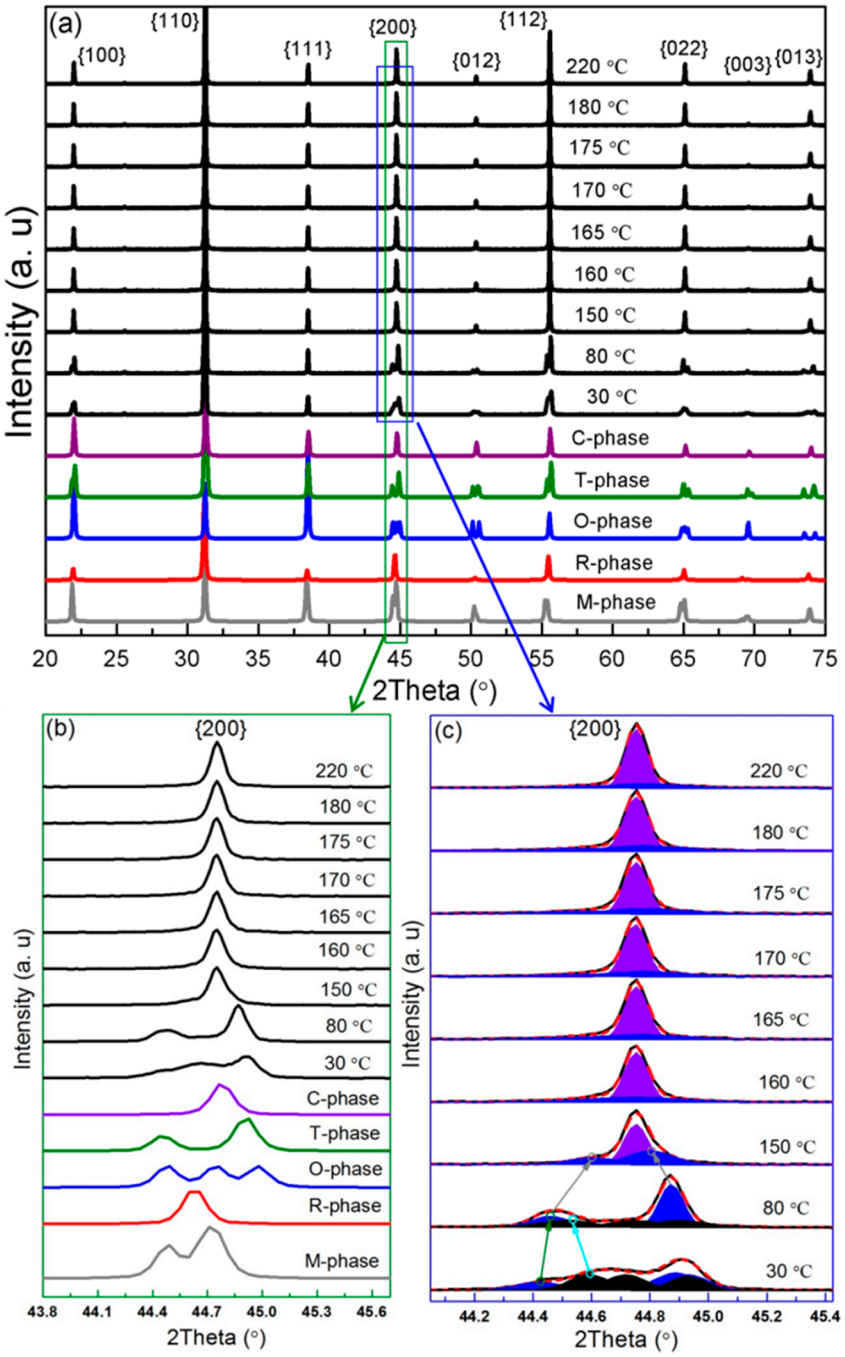

Figure 1. (**a**) The temperature dependent XRD patterns of PZN-9PT single crystals from 30 °C to 220 °C. Simulated XRD patterns (color lines at the bottom of Figure 1a) for pure monoclinic (*Mc*), rhombohedral (*R*), orthorhombic (*O*), tetragonal (*T*) and cubic (*C*) phase of PZN-9PT are also illustrated; (**b**) and (**c**) display the amplified curves around {200} with fitting results.

According to the above discussions, it could be concluded that O-phase and T-phase coexist in PZN-9PT at room temperature. When the temperature increases, O-phase transforms into T-phase firstly, and then transforms into C-phase gradually. In order to provide more detailed information of the phase transition processes, the Gauss and Lorenz functions (8:2) were used to fit the XRD data. Theoretically, for a pure orthorhombic structure, the areas of the three {200} peaks are equal as well as the full width at half maximum (FWHM). But for a pure tetragonal structure with two {002} peaks, one peak area is twice as large as the other, while the FWHM is equal. Then the fitting parameters can be set according to these quantitative relationships. The red dashed lines in Figure 1(c) show the fitting results, where the areas of the orthorhombic, tetragonal and cubic phases are also illustrated. It is clear that the dominant phase at room temperature is O-phase, as shown by the black areas in

Figure 1(c). The peak of O-phase at 44.6° shifts to lower angle with increasing temperatures, which implies c-axis becomes longer when phase transits from orthorhombic to tetragonal phase, as illustrated by the left atomic model in Figure 1(d). Moreover, the two {200} peaks of T-phase tend to merge into a middle angle (shown by gray arrows in Figure 1(c)) with increasing temperatures, suggesting a shortened c-axis and larger a- and b-axis.

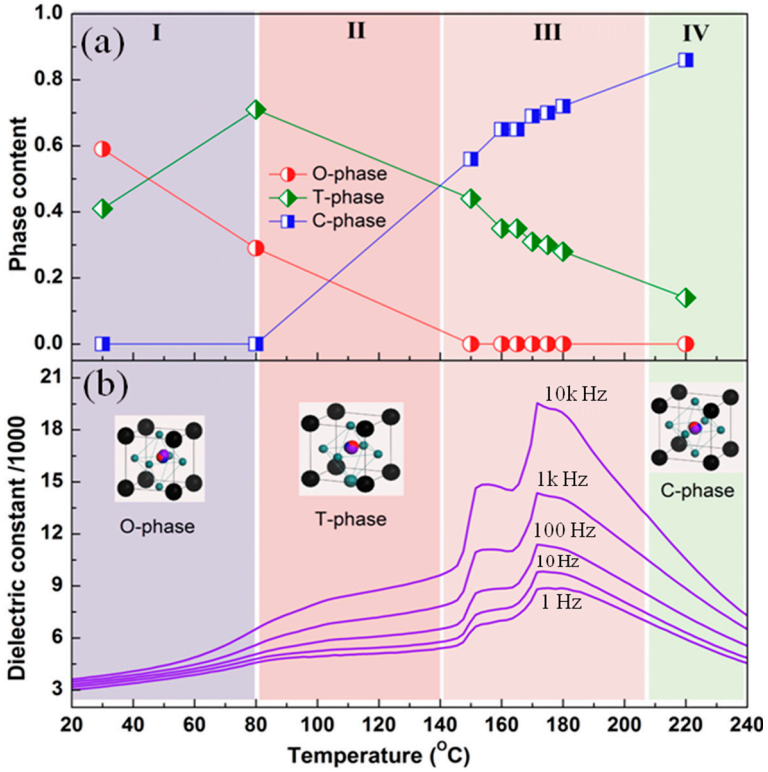

Figure 2. (**a**) The evolution of different phases in PZN-9PT. Four regions with different amount of phases could be clearly distinguished; (**b**) The temperature-dependent of dielectric constant of PZN-9PT at selected frequencies (1, 10, 100, 1k, and 10k Hz).

Based on the fitting data, the phase contents of PZN-9PT at different temperatures could be obtained and illustrated in Figure 2(a). Four easily distinguishable regions can be identified as follows: region I (O- and T-phases coexistence), region II (T-phase dominant), region III (T- and C-phases coexistence), and region IV (C-phase dominant). It can be seen that the content of O-phase decreases with increasing temperature in region I and II, and subsequently becomes nearly zero in region III and IV; T-phase increases in region I, and then decrease gradually in the other regions. From the discussions above, one can conclude that the phase transition in PZN-9PT is a gradual evolution rather than a mutational change with increasing temperature. Due to the change of phases, the dielectric properties of PZN-9PT display a temperature-dependent behavior accordingly, as shown in Figure 2(b). Dielectric curves reveal only weak frequency dispersion in region I, while strong dispersion could be observed with the coexistence of T- and C-phases. It is well known that the relaxor ferroelectrics are characterized by a broad frequency-dependent dielectric peak at radio frequencies, which is associated with the dimensional changes of polar nanoregions (PNRs). By combining 9% ferroelectric PT with PZN relaxor, the structure evolution becomes quite complicated. Upon cooling, some of the C-phase transform into T-phase and then PNRs occur in the crystal. In region III, C-phase is the dominant phase and PNRs grow in size, leading to strong frequency dispersion of dielectric curves. The peak-like behaviors in region III could be attributed to the configuration change of PNRs and/or microdomains. Moreover, in region II, ferroelectric T-phase constitutes a majority and PNRs/microdomains grow into macrodomains which is less sensitive to radio frequencies.

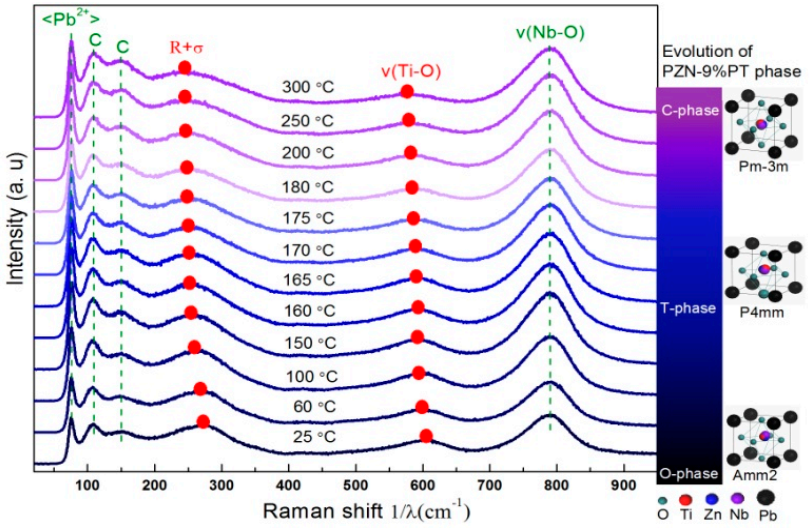

Figure 3. The temperature-dependent Raman spectra of PZN-9PT. Red solid circles show the shifts and intensity changes of the related Ti-O vibration peak. The right image shows a schematic of structure evolution and corresponding atomic models.

Further evidence for the evolution of the phase structures in PZN-9PT can be found from the Raman spectra, which is very sensitive to the change of the structure, symmetry and short range order at nanoscale. As shown in Figure 3, 6 robust active modes could be observed, labeled as <Pb^{2+}>, C, σ and R, <Ti-O>, and <Nb-O>, respectively. These modes are originated from the vibrations of Pb^{2+} cation, coupling between Pb^{2+} and the neighboring entities, B-O bending and ion-covalent BO_6 vibration (B: Ti and Nb), stretching TiO_6 and NbO_6 modes, respectively. One can see that the σ, R and <Ti-O> modes reveal a blue shift as well as a decrement of the peak intensity with increasing temperatures. These results are consistent well with the observations reported by Mishra *et al.* [19] and Cheng *et al.* [20]. The gradual shift of these modes also implies that the structure evolution of PZN-9PT is continuous rather than mutational, in agreement with the XRD results.

2.2. Piezoelectric properties of PZN-9PT crystals

On account of the multi-phase coexistence, PZN-9PT possesses excellent piezoelectric, electromechanical and ferroelectric properties. Figure 4(a) and (b) display the longitudinal mode impedance and phase angle, and the corresponding thickness mode impedance and phase angle at room temperature, respectively. Based on the resonance frequency (f_r) and anti-resonance frequency (f_a), the longitudinal (k_{33}) and thickness (k_t) electromechanical coupling factors are calculated to be 92% and 72%, respectively, by the following equations [21,22]:

$$k_{33}^2 = \frac{f_r}{f_a}\cot\left(\frac{\pi}{2}\frac{f_r}{f_a}\right), \quad (1)$$

and

$$k_t^2 = \frac{\pi}{2}\frac{f_r}{f_a}\tan\left(\frac{\pi}{2}\frac{f_a - f_r}{f_a}\right). \quad (2)$$

These results indicate that the PZN-9PT single crystal exhibit high electromechanical coupling properties. It is also worth noting that the k_t of TSSG-growth PZN-9PT is much superior to the modified Bridgman method [23]. The piezoelectric coefficient d_{33} is measured to be 2350 pC/N by a d_{33} meter. According to the resonance measurement, the d_{33} can be calculated to be 2240 pC/N which is slightly lower than the directly measured value.

Preprints (www.preprints.org) | NOT PEER-REVIEWED | Posted: 1 May 2017 doi:10.20944/preprints201705.0013.v1

Peer-reviewed version available at Crystals 2017, 7, , 130; doi:10.3390/cryst7050130

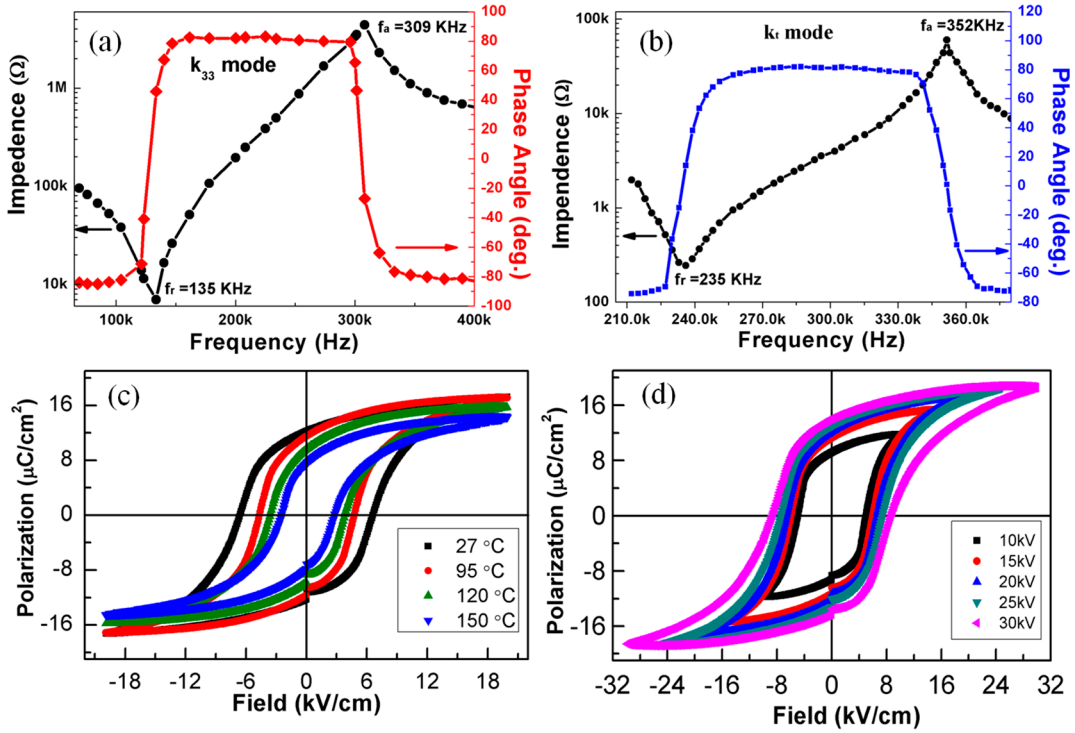

Figure 4. (**a**) Longitudinal impedance and phase angle as a function of frequency based on resonance and anti-resonance frequencies for [001]-oriented bar PZN-9PT crystals. (**b**) Thickness impedance and phase angle as a function of frequency for [001]-oriented square PZN-9PT crystals; (c) and (d) *P-E* loops of [001]-oriented PZN-9PT crystal at different temperatures and electric fields, respectively.

The polarization-electric field (P-E) hysteresis loops of the PZN-9PT crystal were measured as a function of electric field and temperature at 2 Hz, which is shown in Figure 4(c). It can be seen that the coercive field E_c decreases with increase of temperature, but the statured remnant polarization P_r reaches at a maximum at T_{O-T} firstly and then decreases (Figure 4c), which are resulted from flexibility enhancement of domain switching and moving near the T_{O-T}. The statured remnant polarization P_r reaches 20 μC/cm², with a coercive electric field E_c = 9 kV/cm at room temperature (Figure 4d). This evolutions between P_r and temperature indicate that the piezoelectric properties become weak gradually with the phases transition from O-phase to T-phase and to C-phase. It is worth noting that the coercive field E_c of PZN-9PT single crystal is about 2 ~ 3 times larger than that of PMN-33mol%PT, manifesting a more stable domain state in PZN-PT single crystals.

2.3. Nano twin domains of PZN-9PT crystals

One probable explanation for the excellent properties of PZN-PT is the adaptive phase model based on nanoscale twinned O and T domains [24], which is evidenced in this work. The dark field TEM image (Figure 5(a)) shows a large number of domain-like bend striations in the order of several tens angstrom wide, indicating typical relaxor domain structure. Similar domain striations were previously reported by Xu *et al.* [25] in the compositions near the MPB of PMN-*x*PT and designated as tweed-like structures. The selected area electronic diffraction (SAED) pattern captured along pseudocubic [001] zone axis (Figure 5b) shows that the 220 and 2-20 reflections are perpendicular to each other strictly, as illustrated by the blue dashed square. This result implies that the phase of as-grown PZN-9PT neither belongs to monoclinic nor to rhombohedral structure, consistent well with the XRD results. Additionally, single crystal of PZN-9PT exhibit twin structures, as suggested by the red curve line in the upper left of Figure 5b from the profile line of the emission diffraction spot (as marked by the red dashed line in Figure 5b). This result can be further confirmed by the high resolution TEM (HRTEM) images, as shown in Figure 5d, corresponding to the inverse Fast Fourier Transformation (FFT) image from Figure 5c. The average domain size has been estimated to

be about 8.3 nm in width, as labeled by the yellow double arrow in Figure 5d. Probably, the twin structures induce the crystal of PZN-9PT to exhibit the outstanding piezoelectric properties, as demonstrated in Figure 4. Moreover, from the inverse FFT image (Figure 5f) of the blue rectangle area in Figure 5(e), we can calculate the lattice parameters of *a* and *b* for the PZN-9PT crystals to be about 4.05Å and 4.03Å, respectively, which are well consistent with the XRD results (O-phase: a=4.031Å, b=4.05Å; T-phase: a=b=4.036Å). Based on above observations, the correlation between the structure evolution and domain configuration then reveals interesting and important for understanding of the origin of giant piezoelectric response in PZN-PT. The continues behavior of the phase evolution implies that PZN-9PT is in an instable regime, which may be the key factor responsible for its ultrahigh piezoelectric coefficient. Temperature dependent TEM and/or in-situ synchrotron white-beam X-ray microdiffraction analyses [26] should be conducted in the future to establish possible correlations. It is reliably to speculate that the coexistence of T-phase and O-phase results in large amount of nanoscale twin domains, while the coexistence of T-phase and C-phase lead to nanoscale domains (including nano twin domains) and polar nano regions (PNRs) at around Tm and then responsible for the diffuse dielectric peaks.

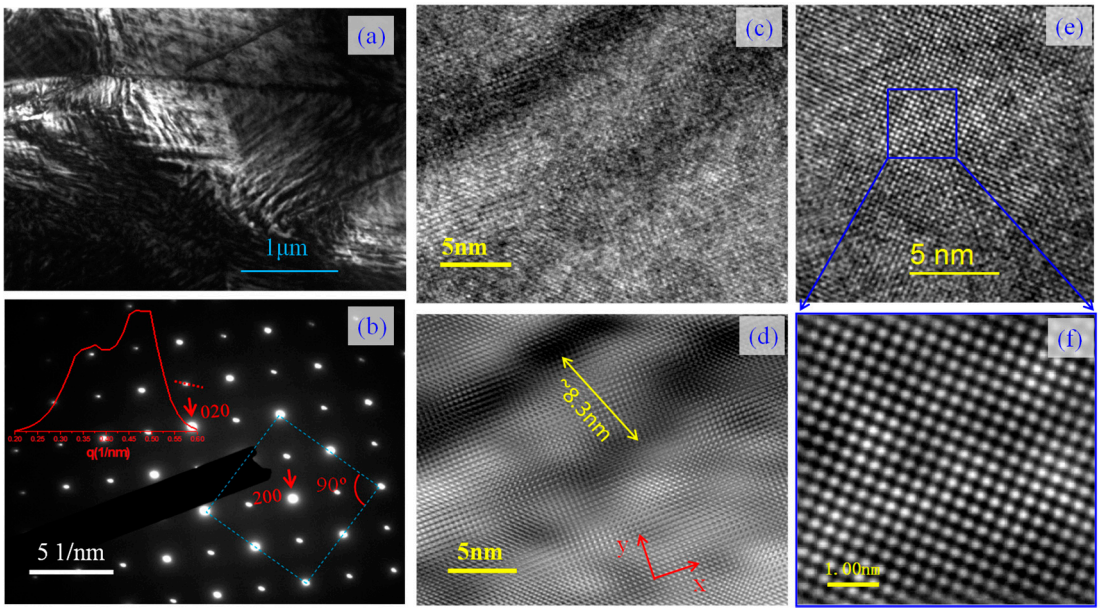

Figure 5. TEM images. (**a**) the low TEM image; (**b**) SAED image; (**c**) and (**e**) high resolution TEM image; (**d**) corresponding to the inverse FFT image of (c); (e) corresponding to the inverse FFT image of the blue rectangle area in Figure 5(**e**).

3. Materials and Methods

***Fabrication of PZN-9PT single crystal*:** The PZN-9PT single crystals were grown by top-seeded solution method. The start materials, PbO (99.9%), TiO_2 (99.9%), ZnO (99.9%), Nb_2O_5 (99.9%), were mixed according to the designed composition of PZN-9PT. Here, 10% of ZnO in excess of stoichiometric ratio mole was added in the mixture to suppress the pyrochlore phase and decrease segregation simultaneously. The mixture of PbO and H_3BO_3 (99.9%) was used as flux. The growing process was similar to the ones described in Refs. [27] and [28]. The weighed chemicals were thoroughly mixed and loaded into a platinum crucible with size of Φ40×50 mm^2, which were then placed into a vertical tube furnace equipped with an automatic temperature controller to melt. The furnace was heated from room temperature to 1050 ºC at a rate of 100 ºC/h, and held for 20 h and then slowly cooled from 1050 ºC to 970 ºC at a rate of 5 ºC/h, and 940ºC to 900 ºC at a rate of 0.5 ºC/h. At the end of a slow cooling process, the as-grown crystal was pulled out of the melt and then annealed to the room temperature at a rate of 20 °C/h.

***Characterization procedure*:** Firstly, the crystal component was analyzed by inductively coupled plasma optical emission spectrometry (ICP-OES). And then in situ high-temperature XRD

data were collected using the D8 Advance (Bruker, Germany) high temperature-diffractometer equipped with Cu-Ka radiation and a graphite monochromator. The scan step is of 0.02^{o} (2θ) with an angular range of 10-70°. The as-grown single crystals were sliced into plates and bars along the [001] direction with different dimensions for the electric measurements. A sample with dimensions of $4^{L}\times4^{W}\times0.5^{T}$ mm^3 was used for dielectric and piezoelectric measurements, and another sample with dimensions of $3.5^{L} \times 2.5^{W} \times 0.6^{T}$ mm^3 for ferroelectric measurements. For resonance and anti-resonance measurements, a sample with dimensions of $0.9^{L}\times0.9^{W}\times3.12^{T}$ mm^3 was prepared. All the samples were polished and coated with silver paste as electrodes. The dielectric properties were measured using a computer-controlled Alpha-A broadband dielectric/impedance spectrometer (Novocontrol GmbH, Germany), with an AC signal of 0.3V (peak-to-peak) applied. Measurements were carried out from -30°C to 300°C with a step of 2°C. The same setup was used to measure the resonance frequency (f_r) and anti-resonance frequency (f_a) of a bar sample. Poling was performed by applying a DC electric field of 15 kV/cm along the [001] direction of the crystal at 120°C for 15 min, and then keeping the electric field on while cooling down to room temperature. Piezoelectric coefficient was measured using a quasi-static d_{33} meter (Institute of Acoustics, Chinese Academy of Sciences, model ZJ-4AN). The polarization-electric field (P–E) hysteresis loop was tested using an aix-ACCT TF2000 analyzer. The microstructure of the crystal sample was studied by TEM (JEOL, JEM-2100F). The out-of-plane feature of the ferroelectric domains was investigated by piezoelectric force microscope (Asylum Research, Oxford).

4. Conclusions

To sum up, the evolution of phase transition of relaxor ferroelectric PZN-9PT from orthorhombic to cubic structure is a continuous process rather than a sharp process, as demonstrated by the variable XRD and Raman spectra. This phenomenon is very similar to the phase transition of paraffin from solid to liquid. Resonance and anti-resonance spectrum show that the PZN-9PT single crystals exhibit excellent piezoelectric properties, which is probably originated from the twin structures in the PZN-9PT single crystal, as demonstrated by the TEM.

Acknowledgments: This work was supported by the Chinese Postdoctoral Science Foundation (No.2015M572356), the National Natural Science Foundation of China (Nos.11604214, 11604140 and 21405106), the Hong Kong, Macao and Taiwan Science & Technology Cooperation Program of China (No.2015DFH10200), and the Science and Technology Research Items of Shenzhen (No.JCYJ20160422102802301 & KQJSCX20160226195624).

Author Contributions: H.Z. and S.K. conceived the idea and designed the experiments; T.L. prepared the PZN-PT single crystals; H.Z., N.Z., M.M., P.L., and C.H. performed the experiments; X.Z., H.H., L.C. and S.K. analyzed the data and wrote the paper; H.H, M.M. and S.K. revised the paper. All authors discussed the results and have given approval to the final version of the manuscript.

Conflicts of Interest: The authors declare no conflict of interest.

References

1. Kuwata, J.; Uchino, K.; Nomura, S. Dielectric and piezoelectric properties of $0.91Pb(Zn_{1/3}Nb_{2/3})O_3$-$0.09PbTiO_3$ single crystals. *Jpn. J. Appl. Phys*. **1982**, *21*, 1298-1302.
2. Zhang, S.J.; Li, F.; Jiang, X.N.; Kim, J.; Luo, J.; Geng, X.C. Advantages and challenges of relaxor-$PbTiO_3$ ferroelectric crystals for electroacoustic transducers – a review. *Prog. Mater. Sci.* **2015**, *68*, 1-66.
3. Sun, E.W. and Cao, W.W. Relaxor-based ferroelectric single crystals: Growth, domain engineering, characterization and applications. *Prog. Mater. Sci.* **2014**, *65*, 124-210.
4. Zhang, S.J. ; Li, F. J..High performance ferroelectric relaxor-$PbTiO_3$ single crystals: status and perspective. *J. Appl. Phys.* **2012**, *111*, 031301.
5. Zhang, S.J. ; Xia, R.; Lebrun, L.; Anderson, D.; Shrout, T.R. Piezoelectric materials for high power, high temperature applications. *Mater. Lett.* **2005**, *59*, 3471-3475.

6. Li, T.; Li, X.Z.; Guo, D.; Wang, Z.J.; Liu, Y.; He, C.; Chu, T.; Ai, L.D.; Pang, D.F.; Long, X.F. Phase diagram and properties of high T_C/T_{R-T} $Pb(In_{1/2}Nb_{1/2})O_3$–$Pb(Zn_{1/3}Nb_{2/3})O_3$–$PbTiO_3$ ferroelectric ceramics. *J. Am. Ceram. Soc*. **2013**, *96*, 1546-1553.
7. Haertling, G.H. Ferroelectric ceramics: history and technology. *J. Am. Ceram. Soc*. **1999**, *82*, 797-818.
8. Samara, G.A. The relaxational properties of compositionally disordered ABO_3 perovskites. *J. Phys - Condens. Matter* **2003**, *15*, R367-R411.
9. Ye, Z.-G. Crystal chemistry and domain structure of relaxor piezocrystals. *Curr. Opin. Solid State Mater*. **2002**, *6*, 35-44.
10. Ye, Z. G. Relaxor ferroelectric complex pervoskites: structure, properties and phase transitions. *Key Engineering Mater*. **1998**, 155, 81-122.
11. Janga, H.M.; Kim, S. C. $Pb(B'_{1/2}B''_{1/2})O_3$-type perovskites: Part I. Pair-correlation theory of order-disorder phase transition. *J. Mater. Res*. **1997**, 12, 2117-2126.
12. Wang, Y.J.; Wang, D.; Yuan, G.L.; Ma, H.; Xu, F.; Li, J.F.; Viehland, D.; Gehring, P.M. Fragile morphotropic phase boundary and phase stability in the near-surface region of the relaxor ferroelectric $(1-x)Pb(Zn_{1/3}Nb_{2/3})O_3$-$xPbTiO_3$: [001] field-cooled phase diagrams. *Phys. Rev. B* **2016**, *94*, 174103.
13. Cox, D.E.; Noheda, B.; Shirane, G.; Uesu, Y.; Fujishiro, K.; Yamada, Y. Universal phase diagram for high-piezoelectric perovskite systems. *Appl. Phys. Lett*. **2001**, *79*, 400-402.
14. He, C.J.; Xu, F.; Wang, J.M.; Liu, Y.W. Refractive index dispersion of relaxor ferroelectric $0.9Pb(Zn_{1/3}Nb_{2/3})O_3$-$0.1PbTiO_3$ single crystal. *Cryst. Res. Technol*. **2009**, *44*, 211-214.
15. Slodczyk, A.; Colomban, P. Probing the nanodomain origin and phase transition mechanisms in (un)poled PMN-PT single crystals and textured ceramics. *Materials* **2010**, *3*, 5007-5028.
16. Ye, Z.-G.; Dong, M.; Zhang, L. Domain structures and phase transitions of the relaxor-based piezo-/ferroelectric $(1-x)Pb(Zn_{1/3}Nb_{2/3})O_3$-$xPbTiO_3$ single crystals. *Ferroelectrics*, **1999**, *229*, 223-232.
17. Chang, W.S.; Lim, L.C.; Yang, P.; Ku, C.-S.; Lee, H.-Y.; Tu, C.-S. Transformation stress induced metastable tetragonal phase in $(93–92)\%Pb(Zn_{1/3}Nb_{2/3})O_3$–$(7–8)\%PbTiO_3$ single crystals. *J. Appl. Phys*. **2010**, 108, 044105.
18. Uesu, Y.; Matsuda, M.; Yamada, Y.; Fujishiro, K.; COX, D.E.; Noheda, B.; Shirane, G. Symmetry of high-piezoelectric Pb-based complex perovskites at the morphotropic phase boundary: I. neutron diffraction study on $Pb(Zn_{1/3}Nb_{2/3})O_3$–$9\%PbTiO_3$. *J. Phys. Soc. Jpn*. **2002**, *71*, 960-965.
19. Mishra, K.K.; Arora, A.K.; Tripathy, S.N.; Pradhan, D. Dielectric and polarized Raman spectroscopic studies on $0.85Pb(Zn_{1/3}Nb_{2/3})O_3$-$0.15PbTiO_3$ single crystal. *J. App. Phys*. **2012**, *112*, 073521.
20. Cheng, J.; Yang, Y.; Tong, Y.H.; Lu, S.B.; Sun, J.Y.; Zhu, K.; Liu, Y.L.; Siu, G.G.; Xu, Z.K. Study of monoclinic-tetragonal-cubic phase transition in $Pb(Zn_{1/3}Nb_{2/3})O_3$–$0.08PbTiO_3$ single crystals by micro-Raman spectroscopy. *J. Appl. Phys*. **2009**, *105*, 053519.
21. IEEE Standard on Piezoelectricity, An American National Standard, The Institute of Electricity and Electronics Engineers, **1979**.
22. Zhang, S.J.; Randall, C.A.; Shrout, T.R. Characterization of perovskite piezoelectric single crystals of $0.43BiScO_3$–$0.57PbTiO_3$ with high Curie temperature. *J. Appl. Phys*. **2004**, *95*, 4291-4295.
23. Harada, K.; Hosono, Y.; Saitoh, S.; Yamashita, Y. Crystal growth of $Pb[(Zn_{1/3}Nb_{2/3})_{0.91}Ti_{0.09}]O_3$ using a crucible by the supported Bridgman method. *Jpn. J. Appl. Phys*. **2000**, *33*, 3117-3120.
24. Jin, Y.M.; Wang, Y.U.; Khachaturyan, A.G.; Li, J.F.; Viehland, D. Conformal miniaturization of domains with low domain-wall energy: monoclinic ferroelectric states near the morphotropic phase boundaries. *Phys. Rev. Lett*. **2003**, 91, 197601.
25. Xu, Z.; Kim, M.; Li, J.F.; Viehland, D. Observation of a sequence of domain-like states with increasing disorder in ferroelectrics. *Philos. Mag. A*, **1996**, *74*, 395-406.
26. Li, T.; Du, Z. H.; Tamura, N.; Lu, W.; Ye, M.; Zeng, X. R.; Ke, S. M.; Huang, H. T. In-situ Synchrotron X-ray Micro-Beam Observation of Phase Transition and Nanotwin Domain Structure in (1-x)PZN-xPT Single Crystals. (In preparation).
27. Long, X. F.; Ling, J.B.; Li, X.Z.; Wang, Z. J.; Ye, Z.-G. Growth and di-/piezoelectric properties of Al-doped PMN-30PT single crystals. *Cryst. Growth Des*. **2009**, *9*, 657-659.
28. Long, X. F.; Ye, Z.-G. Top-seeded solution growth and characterization of rhombohedral PMN–30PT piezoelectric single crystals. *Acta Mater*. **2007**, *55*, 6507-6512.